PAPER

Check for updates

The role of aldehydes on sulfur based-new particle formation: a theoretical study†

Guohua Zhang,‡[a] Min Liu,‡[b] Yaning Han,[b] Zhongteng Wang,[b] Wei Liu, [b]
Ying Zhang*[a] and Jing Xu *[b]

Aldehydes play a crucial role in the formation of atmospheric particles, attracting significant attention due to their environmental impact. However, the microscopic mechanisms underlying the formation of aldehyde-involved particles remain uncertain. In this study, through quantum chemical calculations and molecular dynamics (MD) simulations, we investigate the microscopic formation mechanisms of binary and ternary systems composed of three representative aldehydes, two sulfur-based acids, water, and two bases. Our research findings reveal that the most stable structures of acid-aldehyde clusters involve the connection of acids and aldehyde compounds through hydrogen bonds without involving proton transfer reactions, indicating relatively poor cluster stability. However, with the introduction of a third component, the stability of 18 clusters significantly increase. Among these, in ten systems, acids act as catalysts, facilitating reactions between aldehyde compounds and water or alkaline substances to generate glycols and amino alcohols. However, according to MD simulations conducted at 300 K, these acids readily dissociate from the resulting products. In the remaining eight systems, the most stable structural feature involves ion pairs formed by proton transfer reactions between acids and aldehyde compounds. These clusters exhibit remarkable thermodynamic stability. Furthermore, the acidity of the acid, the nature of nucleophilic agents, and the type of aldehyde all play significant roles in cluster stability and reactivity, and they have synergistic effects on the nucleation process. This study offers microscopic insights into the processes of new particle formation involving aldehydes, contributing to a deeper understanding of atmospheric chemistry at the molecular level.

1. Introduction

New particle formation (NPF) is a key process in the generation of atmospheric secondary organic aerosols (SOA) within the troposphere.[1–4] It has garnered attention for its significant implications on climate and human health.[5–7] NPF involves the initial formation of stabilized clusters from small molecules, which then grow into larger particles.[8] Despite its importance, the chemical identity and significance of vapors, especially in the formation of small nucleated particles (<1 nm), remain uncertain due to technological constraints.

Early experiments at the CLOUD chamber demonstrated NPF from sulfuric acid (H_2SO_4, SA) and bases like ammonia (NH_3, A), methylamine (CH_3NH_2, MA), and dimethylamine (($CH_3)_2NH$, DMA).[9–15] However, their concentrations proved

insufficient to fully elucidate particle nucleation rates and growth rates under atmospheric conditions.[8,16,17] Further research indicates that volatile organic compounds (VOCs) are crucial in both particle formation and growth phases.[18–23]

Among VOCs, aldehydes such as formaldehyde (FA) and α-dicarbonyls like glyoxal (GL) and methylglyoxal (MG) are significant contributors to atmospheric chemistry, with concentrations in the ppb range and an annual production exceeding 185 Tg yr-1. These compounds, primarily generated through oxidative combustion of organic substances, have diverse sources that include urban emissions and biogenic processes.[24–28] In the atmosphere, aldehydes contribute to the formation of free radicals (*e.g.*, HO_x), ozone (O_3), and peroxycarboxylic nitric anhydride (PAN),[29–31] and play a pivotal role in particles formation.[32–39] For example, laboratory studies have shown that gaseous GL can lead to significant particle growth rates,[40] contributing notably to SOA formation in various global locations.[41,42] Model results from the GEOS-chem model suggest that GL and MG are expected to contribute approximately 11 Tg yr-1 to global particles production through irreversible uptake.[43] Additionally, GL and FA have been identified in cloud and fog water, indicating their role in aqueous-phase reactions that contribute to particles formation.[44]

[a]Jinhua Advanced Research Institute, Jinhua, Zhejiang, 321013, P. R. China. E-mail: yzhang1981@sina.com

[b]Department of Optical Engineering, College of Optical, Mechanical and Electrical Engineering, Zhejiang A&F University, Hangzhou, Zhejiang, 311300, P. R. China. E-mail: jingxu@zafu.edu.cn

‡ These authors contributed equally to this work.

SA and methanesulfonic acid (CH_3SO_3OH, MSA) are significant products of Earth's sulfur cycle with high gas-phase concentrations and active atmospheric participation, and have been identified as important drivers of atmospheric particle nucleation.[45-65] Aldehydes and sulfur-containing compounds play a significant role in NPF at the atmosphere–biosphere and atmosphere–hydrosphere interfaces. These compounds significantly influence cloud formation processes and further have implications for global climate patterns.[66] Recent experimental studies indicate that sulfur-based acids can enhance the yield of aldehydes to form particles.[67-71] Yet, there are studies indicating that the combined product of aldehydes and acids alone does not adequately account for the observed particle yields, and kinetic simulations propose that the cluster formation involving aldehyde and acid is almost negligible in terms of growth and formation.[72] Water and basic molecules, like ammonia and small alkyl organic amines, which are prevalent in both gaseous and particulate phases, have been demonstrated to facilitate new particle formation (NPF) through acid–base reactions or oxidation reactions with hydroxyl, ozone, and nitrate.[51,52,54-56,73-79] It is noteworthy that the carbonyl group in aldehydes, characterized by a sp^2 hybridized carbon–oxygen double bond, is particularly susceptible to nucleophilic attack. This interaction can result in the displacement of electrons in the π bond to the more electronegative oxygen atom,[80,81] influencing the mechanism of new particle formation. Given this, nucleophilic agents like water and basic molecules emerge as potential intrinsic drivers in the reaction dynamics of aldehydes and acids. However, the understanding of atmospheric nucleation processes involving aldehydes and acids, particularly in the presence of water or basic molecules, remains limited. Therefore, a comprehensive investigation into NPF driven by aldehydes, acids, water, or basic precursors is imperative to fully elucidate the underlying molecular mechanisms of such nucleation.

In this study, the role of aldehydes in sulfur-based NPF are investigated at a microscopic level. We focus on two types of acids (SA and MSA), three aldehydes (FA, GL, and MG), two bases (A and MA), and water (W). The structures, energies, thermodynamic and dynamic stabilities, and interactions of the most stable structures formed by these components were examined. Furthermore, the mechanism of proton transfer process and the impact of each component on NPF were analyzed. This work contributes to a deeper understanding of the nucleation mechanism of NPF at the molecular level.

2. Theoretical methods

2.1 Clusters structural calculations

In this study, the target systems consist of six binary systems and eighteen ternary systems, incorporating two kinds of acids, three kinds of aldehydes, two kinds of bases, and water. To comprehensively obtain potential initial structures, we employed the ABCluster software[82,83] with the artificial bee colony algorithm[84] to explore local minima on the potential energy surface of each cluster. ABCluster, in combination with quantum chemical calculations, has been successfully used to

obtain the local minima in atmospheric studies.[87-89] Here, each reactant gas was randomly placed in a $4 \times 4 \times 4$ box to generate 1000 initial structures for each system. Due to the huge amount of computation (24×1000), we implemented an economic calculation strategy: initially, 1000 initial structures generated by ABCluster for each system underwent optimization using the PM7 semi-empirical method.[85,86] Subsequently, from the obtained 1000 initial configurations, we selected up to 100 minimal structures within $\Delta E < 10$ kcal mol^{-1} (at PM7 level) for further optimization at the B3LYP/3-21G level.[90-92] Following this, up to 20 lowest-energy isomers were reselected for optimization and vibrational frequency calculations, utilizing the B3LYP functional with Grimme's dispersion correction[93] and a 6-31G(d) basis set. Finally, up to 10 local-minimum structures were chosen for accurate single-point energy and frequency calculations at the MP2/6-311+G(d, p) level,[94-96] and the isomers with the lowest Gibbs free energy (298.15 K) obtained at this level were confirmed as the most stable structures. The final Gibbs free energy (G) was determined using the following approach:

$$G = E_{MP_2} + \Delta G_{thermal} \tag{1}$$

Here, E_{MP_2} represents the single-point energy obtained at the MP2/6-311+G(d, p) level, and $\Delta G_{thermal}$ accounts for thermal corrections to Gibbs free energy, incorporating both entropic and enthalpic contributions at the specified temperature (298.15 K).

To validate the reliability of the relative Gibbs free energies (ΔG) at the MP2/6-311+G(d, p)//B3LYP-D3/6-31G(d) level, we used B3LYP-D3/aug-cc-pVTZ, MP2/aug-cc-pVTZ//B3LYP-D3/6-31G(d) and MP2/6-311+G(d, p) as references for our test calculations on the FA–SA–A system. The test results demonstrated that the isomers predicted to have the lowest Gibbs free energies are consistent across all four methods (see Table S1†). Therefore, considering the balance between computational cost-effectiveness and complexity, the MP2/6-311+G(d, p)//B3LYP-D3/6-31G(d) level is sufficient for qualitatively predicting the lowest-energy ground state structure of each system in this study. Frequency calculations confirmed positive vibrational frequencies for all stable minima. Natural bond orbital (NBO) analysis[97,98] was employed to obtain partial charges (δ). All density functional theory (DFT) geometry optimizations and vibrational frequency calculations were performed using the Gaussian 16 program.[99]

2.2 Molecular dynamic simulations and intermolecular interactions analysis

To assess the thermodynamic stabilities of the obtained clusters, molecular dynamics (MD) simulations were conducted with semi-empirical quantum chemical potentials (PM6)[100-102] using the CP2K package.[103] MD simulations can enrich our understanding by depicting the behavior of clusters in dynamic environments, offering insights beyond static calculations. This method illuminates the role of temperature and molecular interactions in determining stability, providing a more nuanced view of the thermodynamic properties. The simulations were

performed in the gas-phase NVT canonical ensemble with Nose–Hover thermostats.[104,105] For validation, we optimized all the lowest-energy structures at the PM6 level, confirming close agreement with geometries obtained by density functional theory. Each simulation comprised five trajectories, each propagated for 100 picoseconds (ps) with a time step of 1 femtosecond (fs), and the temperature was maintained at $T = 300$ K.

To explore molecular interactions in the clusters, we conducted noncovalent interaction (NCI) analysis.[106] NCI analysis describes the relationship between electron density $\rho(r)$ and reduced density gradient (RDG). RDG(s) is calculated by eqn (2) to demonstrate the deviation from the homogeneous distribution of electrons.

$$s = \frac{1}{2(3\pi^2)^{1/3}} \frac{|\nabla\rho|}{\rho^{4/3}} \tag{2}$$

where ρ is the electron density based on MP2/6-311+G(d, p)//B3LYP-D3/6-31G(d), ∇ is the gradient operator, and $|\nabla\rho|$ is the electronic density gradient mode. Multiwfn[107] and VMD[108,109] programs were utilized for RDG-sign(λ_2)ρ scatter plots and bonding isosurface plots, respectively, visualizing the location, strength, and type of weak interactions in the structure. The strength of the interaction was judged by the value of sign(λ_2)ρ, with values close to zero indicating weak interactions, such as van der Waals forces. Negative sign(λ_2)ρ values corresponded to hydrogen bonds (HB), while positive values indicated steric hindrance.

3. Results and discussions

In this study, two types of acids (SA and MSA), three aldehydes (FA, GL, and MG), two bases (A and MA), and water (W) are involved, with investigations focusing on acid-aldehyde systems, both with and without the presence of a base or water. To facilitate comparison across these systems, a simplified naming convention was adopted: X–Y denotes binary systems, and X–Y–Z indicates ternary systems. Here, X represents an aldehyde, Y signifies an acid, and Z corresponds to water or a base. Note that the naming convention used merely reflects the reactants involved and is not indicative of the composition of the resulting products. For instance, the binary system FA–SA is composed of FA and SA as reactants. Similarly, the ternary system FA–SA–W includes FA, SA, and water molecules as reactants. It is worth mentioning that for three-component reactions, all three gas molecules are introduced as reactants simultaneously.

3.1 Acid-aldehyde

To microscopically reveal the role of aldehydes in sulfur-based NPF, three representative aldehydes—mono-carbonyl aldehyde FA, and di-carbonyl aldehydes GL and MG—as well as two representative sulfur-based acids, namely SA and MSA, were considered in this work. The most stable structures identified for different aldehydes and sulfur-based acids in a 1 : 1 ratio at the MP2/6-311+G(d, p)//B3LYP-D3/6-31G(d) level are presented in Fig. 1, with additional high-energy isomers shown in Fig. S1 and S2.† For these most stable acid-aldehyde clusters, the oxygen atoms on the carbonyl groups of all aldehydes form OH⋯O hydrogen bonds with the hydroxyl hydrogen atoms on the SA or MSA molecules, and no proton transfer was observed in any of the systems. The bond length of hydrogen bonds ranges from 1.70 to 1.78 Å. Notably, SA systems exhibit slightly shorter hydrogen bond lengths than MSA systems. NBO analysis reveals that acidic molecules in all acid-aldehyde clusters have a small negative partial charge (δ), while aldehydes have a positive partial charge, indicating a very weak donor–acceptor interaction.

To explore the intermolecular interactions of these acid-aldehyde clusters, NCI analysis was performed on the global
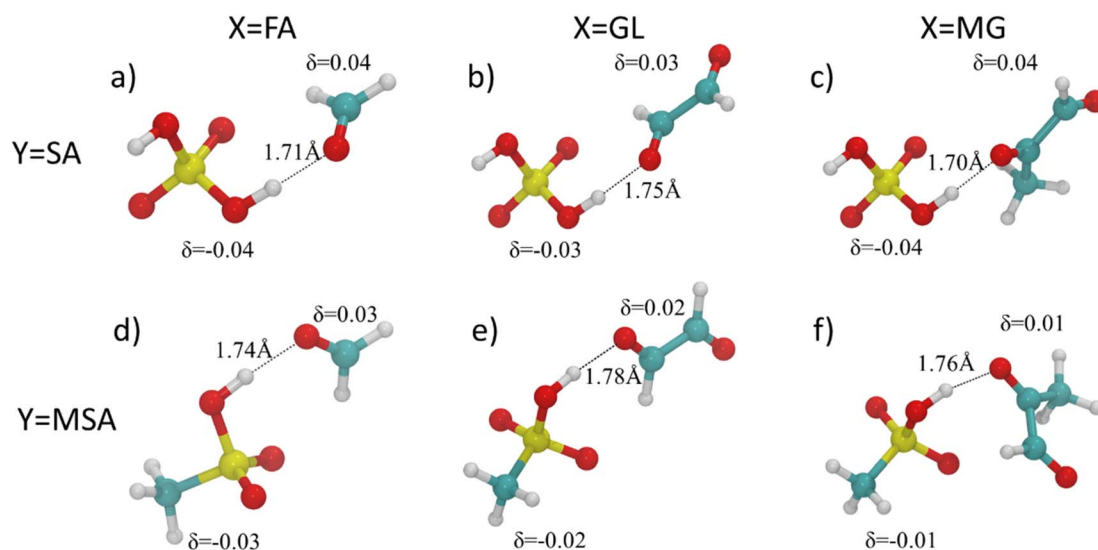

Fig. 1 The most stable structures of X–Y (X = FA/GL/MG; Y = SA/MSA) systems at the level of MP2/6-311+G (2d, 2p)//B3LYP-D3/6-31G(d). Yellow, red, green and white spheres represent sulfur, oxygen, carbon and hydrogen atoms, respectively.
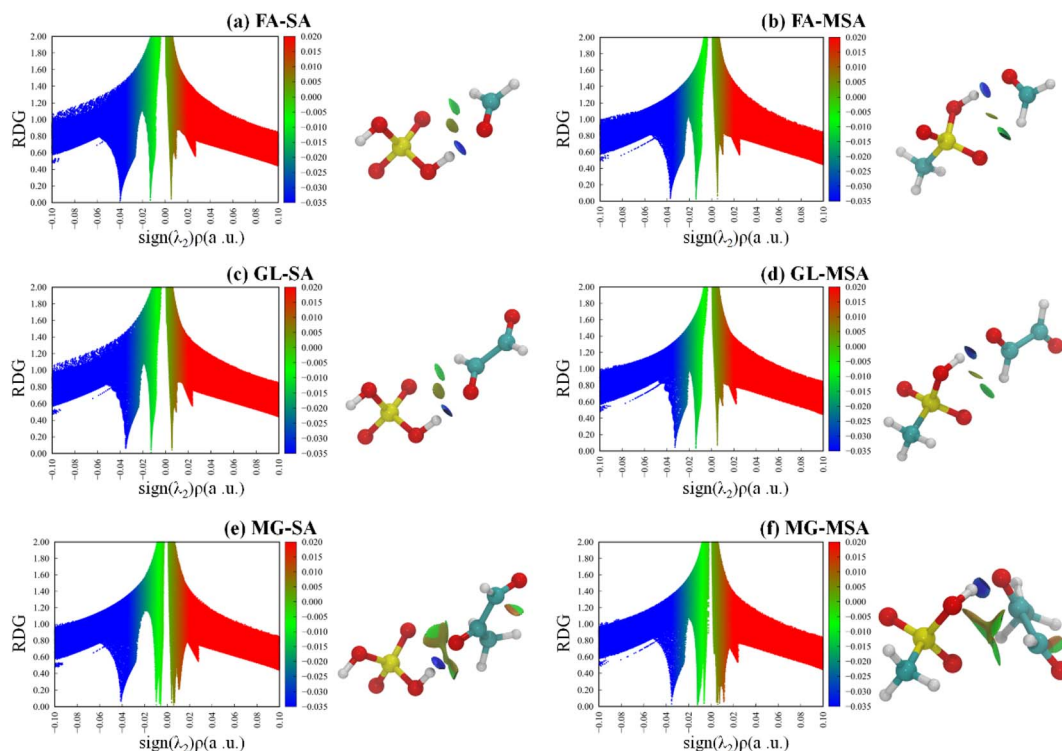
Fig. 2 The plots of RDG *versus* sign(λ_2)ρ function and the visualized bonding isosurfaces for the most stable acid–aldehyde clusters.

minima of these clusters. Fig. 2 illustrates the scatter plot of RDG(s) *vs.* sign(λ_2)ρ, along with corresponding bonding iso-surfaces. The results indicate that all hydrogen-bonded acid-aldehyde clusters exhibit negative sign(λ_2)ρ values, signifying the presence of hydrogen bonds (HBs). The OH···O hydrogen bond positions of all clusters can be identified from the bonding isosurfaces in the blue region. Additionally, van der Waals forces (sign(λ_2)$\rho \sim 0$) and steric hindrance (sign(λ_2)$\rho > 0$) are observed in each cluster. As the molecular weight of the system increases, the van der Waals effect and steric hindrance effect within the composite structure are enhanced. Importantly, the value of sign(λ_2)ρ corresponding to the spike in the SA-based cluster is smaller than that in the MSA-based cluster, indicating a stronger hydrogen bonding attraction formed by aldehyde and SA. These results are further supported by the visual bonding isosurfaces, with all hydrogen bonds corresponding to the structures in Fig. 1 through the disc-like iso-surface. MG-involved systems exhibit more pronounced van der Waals and steric hindrance effects. It is noteworthy that SA systems display shorter hydrogen bond lengths, more pronounced negative partial charges, and sign(λ_2)ρ values in comparison to MSA systems. These findings collectively imply a stronger interaction in binding aldehydes within SA systems than in MSA systems.

The stability of acid-aldehyde clusters was further assessed through thermodynamic analysis and MD simulations. First, dissociation energies of these clusters were calculated at the MP2/6-311+G(d, p)//B3LYP-D3/6-31G(d) level. The binding energies (ΔE), electron energies with zero-point correction (ΔE + ZPE), and corresponding free energies (ΔG) at 298.15 K were listed in Table 1, and dissociation energies were calculated using eqn (3).

$$\Delta G = \sum G(\text{product}) - \sum G(\text{reactant}) = \\ \sum \nu_B G(B) - G(\text{global minima}) \quad (3)$$

As shown in Table 1, the calculated results indicate that FA–SA exhibits a small positive $D_{\Delta G}$ value (0.39 kcal mol^{-1}), while the remaining systems have negative values ranging from -0.21 to -1.63 kcal mol^{-1}. These negative $D_{\Delta G}$ values mean that these clusters tend to dissociate and are thermodynamically unstable. The order of thermodynamic stability is FA > MG > GL for the SA system, while FA > GL > MG for the MSA system. Additionally, most SA systems exhibit smaller dissociation energies than the corresponding values for MSA, aligning with the observed shorter hydrogen bonds and stronger interactions in SA. Next, MD simulations for the six clusters were conducted at 300 K. The MD results reveal that the OH···O hydrogen bond breaks in a very short time, approximately 10 ps for SA and 3 ps for MSA, leading to complete separation of the aldehyde and acid components (see Fig. S3†). The change in energy following hydrogen bond dissociation is predominantly attributed to the contribution of the hydrogen bonds. This indicates that clusters are prone to dissociation to monomers, demonstrating insta-bility at room temperature.

Based on the obtained results, the acid-aldehyde clusters are characterized by a single hydrogen bond between the hydroxyl group on the acid and the oxygen atom in the aldehyde carbonyl group, with no proton transfer process observed. These clusters

Table 1 Dissociation energies (in kcal mol^{-1}) of the acid–aldehyde clusters calculated from the binding energies ($D_{\Delta E}$), electron energies with zero-point corrected ($D_{\Delta E+ZPE}$), and corresponding free energies ($D_{\Delta G}$) at the MP2/6-311+G(d, p)//B3LYP-D3/6-31G(d) level of theory. Positive values mean endothermic and negative values mean exothermic

Dissociation paths	$D_{\Delta E}$	$D_{\Delta E+ZEP}$	$D_{\Delta G}$	Proton transfer	Types of proton transfer
FA–SA → 1*FA +1*SA	10.12	9.64	0.39	No	— —
MG–SA → 1*MG +1*SA	10.72	10.03	−0.21	No	— —
GL–SA → 1*GL +1*SA	9.20	8.36	−0.63	No	— —
FA–MSA → 1*FA +1*MSA	9.02	8.57	−0.72	No	— —
GL–MSA → 1*GL +1*MSA	8.40	7.60	−1.55	No	— —
MG–MSA → 1*MG +1*MSA	10.01	9.37	−1.63	No	— —

exhibit poor thermodynamic stability, consistent with previous studies. Aldehydes exhibit stronger interactions with SA than with MSA, resulting in shorter hydrogen bonds, smaller dissociation free energies, and shorter separation times. This behavior may be attributed to the stronger acidic nature of SA.

3.2 Acid-aldehyde with water or base

Continuing from the analysis of unstable acid-aldehyde clusters, we further investigated ternary X–Y–Z systems, and revealed the role of each component within them. In this context, the third component Z included water (W) and two different alkaline bases NH$_3$ (A) and MA.

3.2.1 Structure. First, when Z is water, the most stable structures of FA/GL/MG–SA/MSA–W systems are depicted in Fig. 3, with additional structures of higher energy shown in Fig. S4 and S5.† These most stable clusters exhibit an eight-membered ring structure where two fragments are connected by two hydrogen bonds. One fragment comprises the acid, while the other consists of the geminal-diol. The two hydrogen bonds connect the two hydroxyl groups in the geminal-diol with the oxygen atom and the hydroxyl hydrogen atom on the acid, with

bond lengths ranging from 1.83 to 1.90 Å and 1.59 to 1.66 Å, respectively. Similar to the acid-aldehyde systems, no proton transfer occurs between the acid and aldehyde here, supported by small δ values (−0.02 ∼ −0.05) in SA or MSA. The geminal-diol is formed by the reaction of aldehyde and water, where water loses one proton to form an alcohol group. Because FA/GL/MG have a carbon end of the carbonyl double bond that is electrophilic due to bond polarity created by resonance, when directly attacked by a nucleophile, the π bond is broken to form an alkoxide intermediate, which is then protonated to yield the alcohol derivative.[80,81] However, water is a weak nucleophile, and the carbonyl carbon usually needs to be activated. Previous studies have shown that the carbonyl group is protonated under acidic conditions, increasing the polarity of the carbonyl bond and making the carbon more electrophilic.[110] Hence, in the presence of water, SA/MSA acts as a catalyst to activate the carbonyl carbon, facilitating the formation of geminal-diol. The mechanism of geminal-diol formation and the specific proton transfer situations are detailed below.

Next, we discuss the systems when the third component Z is either A or MA. Previous studies have demonstrated that basic molecules such as ammonia or small alkylamines not only form
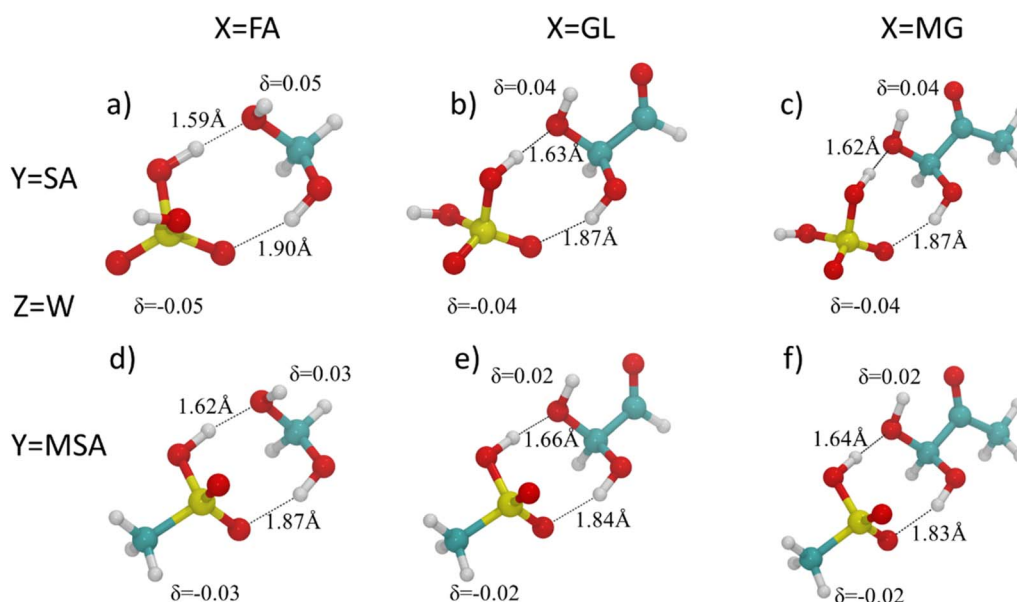

Fig. 3 The most stable structures of X–Y–Z (X = FA/GL/MG; Y = SA/MSA; Z = W) systems at the MP2/6-311+G(d, p)//B3LYP-D3/6-31G(d) level. Yellow, red, green and white spheres represent sulfur, oxygen, carbon and hydrogen atoms, respectively.

atmospheric clusters with higher stability and nucleation rates with SA or MSA but also act as nucleophiles attacking the carbonyl functional groups in aldehydes. Fig. 4 illustrates the geometry of the most stable clusters formed by the reaction of three aldehydes with SA or MSA and basic nucleophilic components, including A and MA molecules, with other high-energy structures displayed in Fig. S6–S9.† These 12 clusters exhibit global minimum structures with an eight-ring-like configuration and two hydrogen bonds. When SA is the acid, a proton is transferred from SA to the aldehyde carbonyl, resulting in an ion pair. As a result, SA with a lost proton exhibits high partial charge values, $\delta = -0.87$ to -0.88. For A or MA, nitrogen of base forms a C–N bond with the aldehyde carbonyl, and the hydrogen on nitrogen forms an O···H–N hydrogen bond with the acid. Clearly, when SA is present, the carbonyl group is protonated, increasing the polarity of the carbon–oxygen double bond and making it more electrophilic. Notably, hydrogen bonds in basic systems are shorter than those in water-based clusters, indicating stronger interactions in base-based systems. When MSA is the acid, two different scenarios exist. Only for FA–MSA–MA and MG–MSA–MA, MSA systems exhibit the same bonding mode as SA systems, with evident proton transfer occurring between the acid and aldehyde. For the remaining four systems (GL–MSA–MA and FA/GL/MG–MSA–A), the bonding mode is similar to that in the presence of water, where MSA, acting as a catalyst, does not undergo changes, while the base loses a proton and forms an aminoalcohol with the aldehyde. Regardless of whether the nucleophile is water or a base, for clusters in which no proton transfer occurs between the acid and aldehyde, SA or MSA still possesses small negative δ values.

To gain a deeper understanding of the formation of compounds in which no proton transfer occurs, further
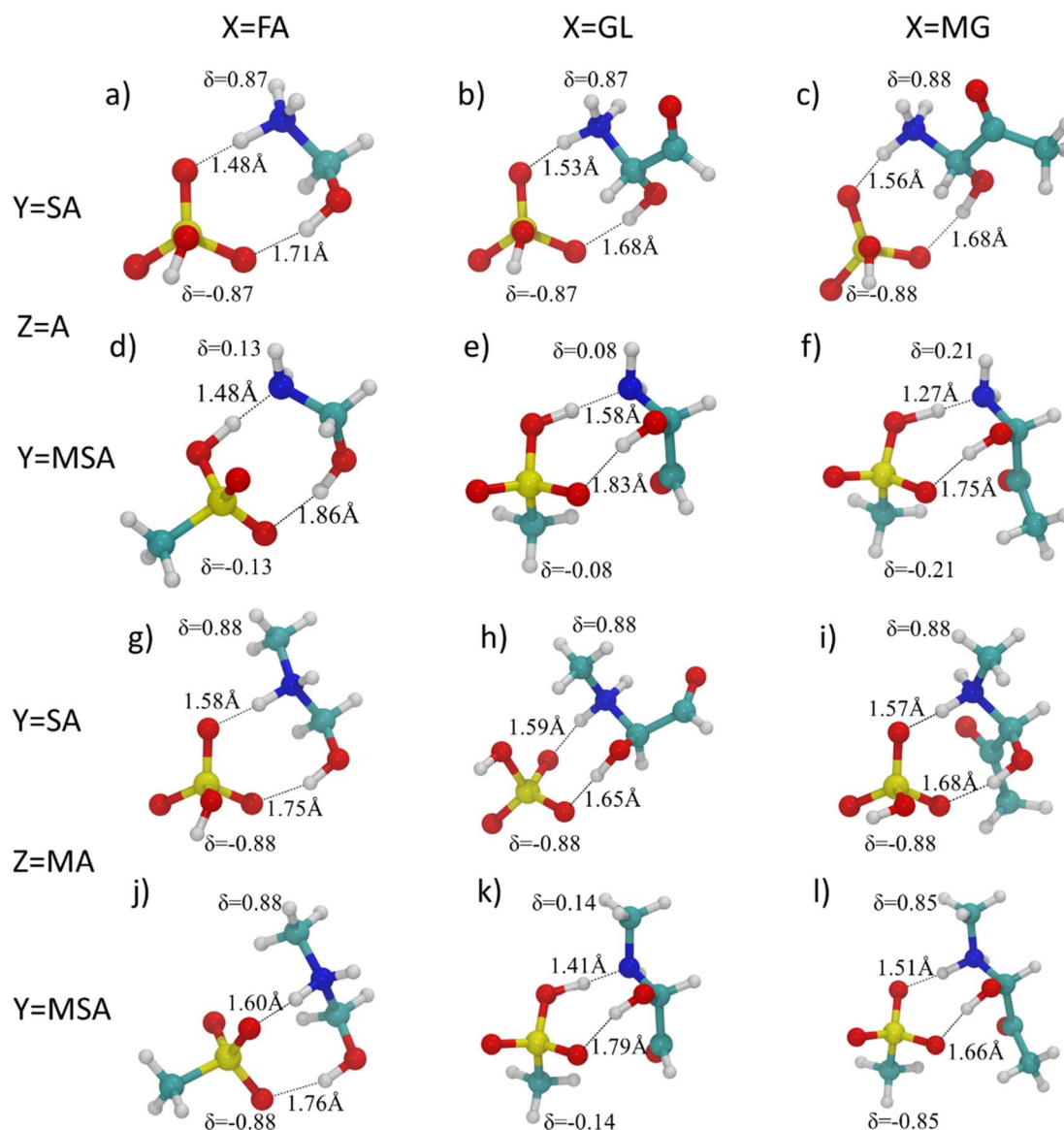

Fig. 4 The most stable structures of X–Y–Z (X = FA/GL/MG; Y = SA/MSA; Z = A/MA) systems at the MP2/6-311+G(d, p)//B3LYP-D3/6-31G(d) level. Yellow, red, blue, green and white spheres represent sulfur, oxygen, nitrogen, carbon and hydrogen atoms, respectively.

investigation into the mechanism of such reactions was conducted. Using 1FA–1MSA–1A as a representative system, transition state calculations for trimolecular reactions were performed, and a complete reaction pathway was constructed. Fig. 5 presents the Gibbs free energy change diagram for the transition among four isomers in the FA–MSA–A system. It also includes the geometric parameters of the corresponding structures, featuring four isomers (iso-1, iso-2, iso-3, iso-4) and two transition states (TS-1, TS-2). From this pathway diagram, it can be seen that in the reactants of the trimolecular reaction, a hydrogen bond interaction with a bond length of 1.53 Å is involved between FA and MSA molecules, while the A molecule is only weakly linked to MSA and FA through a van der Waals interaction. With an activation energy barrier of 2.59 kcal mol^{-1} reaching transition state TS1, it can be observed that the hydrogen atom H_c of MSA is transferred to the oxygen atom O_b of FA, while ammonia is added to the carbon atom C_a in formaldehyde. This results in the formation of an eight-membered ring product (iso-2) containing a stable ion pair. The bond distances are $H_cO_d = 1.72$ Å, $C_aN_h = 1.54$ Å, and $H_iO_j = 1.51$ Å, respectively. Subsequently, this product easily undergoes a barrier-free reaction, involving a second proton transfer via iso-2, TS2, and iso-1 in the current eight-ring model. In this process, the hydrogen atom H_i on the base A migrates to MSA, ultimately forming the global minimum structure iso-1 with the lowest relative energy (ΔG). This product involves two hydrogen bond interactions, with bond distances of $H_cO_d = 1.86$ Å and $N_hH_i = 1.48$ Å, respectively.

According to reaction potential energy surface, we conclude the following reaction mechanism for X–Y–Z systems in which

no proton transfer occurs, and the detailed process is shown in Fig. 5: (1) SA/MSA protonates the carbonyl oxygen, making the carbonyl carbon more electrophilic. After protonation, the oxygen becomes positively charged, representing another resonance form of carbocation. (2) Under acidic conditions, W/A/MA acts as a nucleophile and forms a single bond with the electrophilic carbon. This pushes the two electrons in the carbonyl π bond onto the electronegative oxygen. The oxygen from the carbonyl becomes neutral, while the oxygen/nitrogen from W/A/MA nucleophile becomes positively charged. (3) HSO_4^- or $CH_3SO_3^-$ acts as a base to extract a proton from the neutrally charged W/A/MA, thereby regenerating SA/MSA. Hence, SA/MSA ultimately acts as a catalyst throughout the entire reaction. In fact, for systems in which proton transfer between the acid and aldehyde does occur (FA/GL/MG–SA–A/MA), the reaction is similar to that of TS-1, generating iso-2. SA-based and MSA-based reactions differ in the subsequent step, which may be attributed to the stronger basicity of $CH_3SO_3^-$ compared to HSO_4^-. $CH_3SO_3^-$ is more effective in deprotonating the nitrogen atom in A or MA to form a positively charged ammonolysis product.

3.2.2 Intermolecular interactions. The intermolecular interactions within the most stable clusters of X–Y–Z systems were further examined through NCI analysis. In all systems, the positions of spikes on the scatter plot (RDG vs. sign(λ_2)ρ function) and the bonding isosurfaces visualized on the cluster structures perfectly match in color. Taking six systems containing FA as an example, we illustrate NCI analysis in Fig. 6. It is evident that all systems exhibit two different types of hydrogen bonds, corresponding to two negative sign(λ_2)ρ peaks
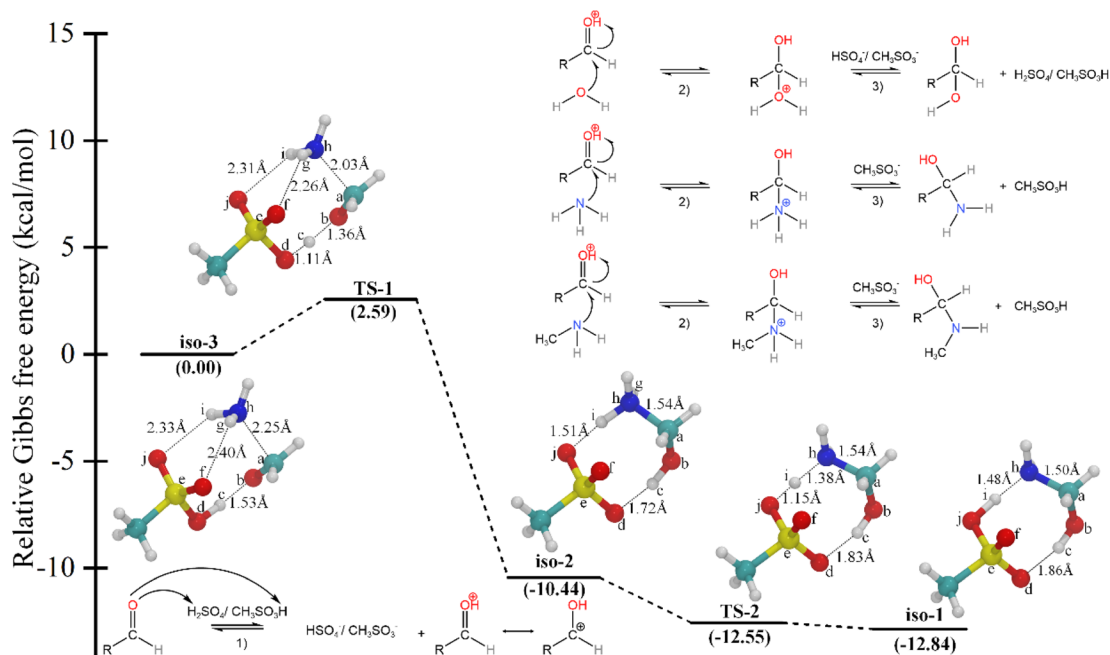

Fig. 5 The Gibbs free energy change diagram for the transition among four isomers in the FA–MSA–A system at the MP2/6-311+G(d, p)//B3LYP-D3/6-31G(d) level of theory (in kcal mol^{-1}). The values in parentheses represent the relative Gibbs free energy values of the isomers or transition states relative to the zero point.
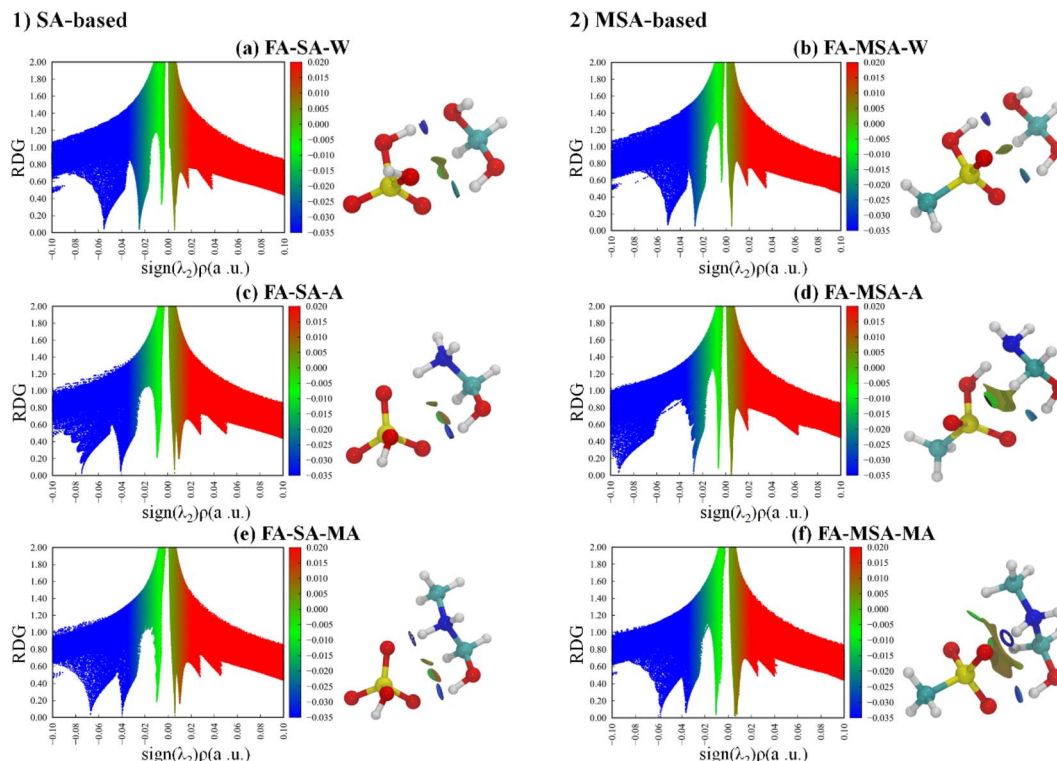
Fig. 6 The plots of RDG *versus* sign(λ_2)ρ function and the visualized bonding isosurfaces for the most stable structures of X–Y–Z (X = FA) clusters.

on the scatter plot. Additionally, van der Waals forces (sign(λ_2)ρ $\sim$ 0) and steric hindrance (sign(λ_2)ρ > 0) are also present in these eight-ring-like ternary systems. Similar patterns are observed for the di-carbonyl aldehydes GL and MG (see Fig. S10 and S11†). These results are also supported by visual bonding iso-surfaces, with all hydrogen bonds corresponding to the structures in Fig. 3 and 4 through disk-shaped isosurfaces. Comparing the interaction positions in the clusters containing mono- and di-carbonyl aldehydes, we observed that only in the GL and MG-based clusters, there are elliptical isosurfaces in half-green and half-orange-red between the attacked carbonyl carbon atom and the free carbonyl functional group. These elliptical isosurfaces correspond to the dual impact of van der Waals effects and mutual exclusion effects. This phenomenon may be attributed to the presence of strong electron-withdrawing groups such as –CHO and –COR in the complex product of GL and MG. In summary, the NCI analysis reveals the presence of various intermolecular interactions within the clusters, including hydrogen bonds, van der Waals forces, and steric hindrance. These interactions play a crucial role in stabilizing the these clusters and influencing their properties and behavior.

3.2.3 Stability. The above results have indicated that acid-aldehyde clusters have poor stability, however, in the presence of nucleophilic molecules such as water or bases, aldehydes can be protonated by the acid or nucleophilic molecules, forming more stable eight-membered ring structures. To confirm the stability of the most stable structures in the X–Y–Z systems, we

investigated the dissociation process of the obtained 18 clusters and calculated their dissociation energies and the corresponding proton transfer reactions.

As shown in Table 2, it is observed that, except for FA–MSA–W (-0.31 kcal mol^{-1}), the $D_{\Delta G}$ values of the dissociation pathways for all other systems are positive (ranging from 0.1 to 15.59 kcal mol^{-1}), indicating that these clusters are not prone to dissociation reactions thermodynamically. Clearly, the third component can effectively improve the stability of acid-aldehyde clusters. This enhanced stability can be attributed to several factors: (1) protonation of aldehydes: in X–Y–Z systems, the carbonyl functional group of aldehydes is protonated by SA or MSA, making the carbon atoms more electrophilic and thus more prone to addition reactions with nucleophilic molecules. (2) Contribution of water or alkali molecules: the presence of water or alkali molecules is crucial for stabilizing the X–Y–Z system. They can form stable hydrolysis or ammonolysis products with aldehydes and provide an additional pair of hydrogen bonds with SA or MSA, enhancing the intermolecular interactions within the cluster.

Furthermore, the effects of different components on $D_{\Delta G}$ were analyzed systematically: (1) aldehydes: clusters composed of di-carbonyl aldehydes (GL and MG) exhibited larger $D_{\Delta G}$ values than those of mono-carbonyl aldehyde (FA), indicating that the complexes generated by hydrolysis or ammonolysis were more stable. Di-carbonyl aldehydes have strong electron-withdrawing groups, which increase the electrophilicity of the carbonyl carbon atom and enhance their ability to accept

Table 2 Dissociation energies (in kcal mol^{-1}) of the most stable clusters in X–Y–Z systems calculated from the binding energies ($D_{\Delta E}$), electron energies with zero-point corrected ($D_{\Delta E+ZPE}$), and corresponding free energies ($D_{\Delta G}$) at the MP2/6-311+G(d, p)//B3LYP-D3/6-31G(d) level of theory, and the details of proton transfer in each cluster. Positive values mean endothermic and negative values mean exothermic

Dissociation paths	$D_{\Delta E}$	$D_{\Delta E+ZEP}$	$D_{\Delta G}$	Proton transfer	Types of proton transfer	
MG–SA–MA → 1*MG + 1*SA + 1*MA	40.31	40.34	15.59	Yes	SA → MG	
GL–SA–MA → 1*GL + 1*SA + 1*MA	38.54	38.71	14.69	Yes	SA → GL	
FA–SA–MA → 1*FA + 1*SA + 1*MA	30.01	43.61	13.94	Yes	SA → FA	
MG–MSA–MA → 1*MG + 1*MSA + 1*MA	29.52	47.44	13.24	Yes	MSA → MG	
GL–MSA–MA → 1*GL + 1*MSA + 1*MA	29.71	45.58	12.61	Yes	MSA → GL	MA → MSA
FA–MSA–MA → 1*FA + 1*MSA + 1*MA	34.29	34.89	10.94	Yes	MSA → FA	
MG–SA–A → 1*MG + 1*SA + 1*A	30.55	31.16	7.96	Yes	SA → MG	
GL–SA–A → 1*GL + 1*SA + 1*A	29.25	29.94	7.48	Yes	SA → GL	
MG–MSA–A → 1*MG + 1*MSA + 1*A	23.06	39.56	7.12	Yes	MSA → MG	A → MSA
GL–MSA–A → 1*GL + 1*MSA + 1*A	21.92	36.99	6.63	Yes	MSA → GL	A → MSA
FA–SA–A → 1*FA + 1*SA + 1*A	27.35	28.38	6.33	Yes	SA → FA	
FA–MSA–A → 1*FA + 1*MSA + 1*A	20.11	33.42	5.74	Yes	MSA → FA	A → MSA
MG–SA–W → 1*MG + 1*SA + 1*W	15.01	31.15	0.57	Yes	SA → MG	W → SA
FA–SA–W → 1*FA + 1*SA + 1*W	15.45	27.79	0.44	Yes	SA → FA	W → SA
GL–SA–W → 1*GL + 1*SA + 1*W	14.88	29.27	0.30	Yes	SA → GL	W → SA
MG–MSA–W → 1*MG + 1*MSA + 1*W	14.01	30.99	0.14	Yes	MSA → MG	W → MSA
GL–MSA–W → 1*GL + 1*MSA + 1*W	21.49	22.16	0.10	Yes	MSA → GL	W → MSA
FA–MSA–W → 1*FA + 1*MSA + 1*W	20.39	21.41	−0.31	Yes	MSA → FA	W → MSA

nucleophiles. (2) Nucleophiles: the $D_{\Delta G}$ values of the clusters formed by different nucleophiles attacking carbonyl carbocations are consistent with their nucleophilicity, with the stability in descending order: $D_{\Delta G}$ (MA-based) > $D_{\Delta G}$ (A-based) > $D_{\Delta G}$ (W-based). This suggests that the stability of the clusters formed by aldehydes under the action of SA or MSA is closely related to the nucleophilicity of the nucleophile. (3) Acid effect: the ΔG values of all SA-based clusters (including X–Y and X–Y–Z systems) are higher than those of the corresponding MSA-based clusters, indicating that SA-based clusters are more thermodynamically stable. This is mainly because SA has a higher acid strength and can better stabilize the partial negative charge of the oxygen atom on the C=O in the aldehyde.

Additionally, MD simulations were performed for all X–Y–Z clusters to evaluate their stability at room temperature (300 K), and the results are shown in Fig. S12–S14.† In systems where no proton transfer occurs between acid and aldehyde in the most stable structures, the acid tends to dissociate from the structure rapidly. Conversely, systems that experienced proton transfer from acid to aldehyde demonstrated enhanced stability, characterized by minimal energy fluctuations and intact components.

In summary, for the three-component reaction, both the acid and nucleophilic reagents play synergistic roles in the reaction with aldehydes, and the acidity of the acid, strength of the nucleophile, and type of aldehyde all contribute to the stability and reactivity of the clusters. Crucially, proton transfer between acid and aldehyde emerges as a vital factor for evaluating cluster stability.

4. Conclusion

Utilizing quantum chemical calculations and MD simulations, we systematically investigated NPF involving three types of aldehydes, two acids, and two bases or water. Our study reveals that acid-aldehyde (X–Y) clusters are merely linked by hydrogen bonds between the acids and aldehydes, without any proton

transfer. Calculations of dissociation energy and MD suggest that these clusters are less thermodynamically stable. The order of thermodynamic stability for SA system is formaldehyde (FA) > methylglyoxal (MG) > glyoxal (GL), while for MSA system, it is FA > GL > MG. When a third component Z (water and base) is present, the most stable structure forms an eight-membered ring *via* two hydrogen bonds, with X–Y–Z systems exhibiting improved stability compared to X–Y systems. Among them, ten systems (FA/GL/MG–SA/MSA–W, FA/GL/MG–MSA–A, GL–MSA–MA) occur twice proton transfer, *i.e.*, MSA → aldehyde and water or base → MSA, resulting in MSA as a catalyst in this process. For the remaining eight clusters (FA/GL/MG–SA–A/MA, FA/MG–MSA–MA), the most stable structures are ion pairs formed by proton transfer from the acids to aldehydes, *i.e.*, acid → aldehyde. These clusters maintain excellent thermodynamic stability. Additionally, under acidic conditions, the electrophilicity of carbon atoms in FA, GL, and MG is progressively enhanced, along with the increasing stability of the formed cluster. With the increase of the acidity of acid and the basicity of the nucleophile, stabilities of products formed in the aldehyde-involved reactions also increase. In summary, this study provides valuable insights into NPF. Proton transfer between acids and aldehydes and the involvement of water/base molecules are crucial for nucleophilic reactions leading to stable nucleated clusters. Additionally, the acidity of the acid, the nature of nucleophilic agents, and the type of aldehyde all play significant roles in cluster stability and reactivity, and they have synergistic effects on the nucleation process. This research not only advances our understanding of aldehydes-based NPF processes but also offers useful guidance for future related studies.

Author contributions

GZ: investigation, methodology, visualization, formal analysis, and writing – original draft. ML: formal analysis, investigation,

methodology, and writing – original draft. YH: methodology, data curation. ZW: visualization. WL: funding acquisition. YZ: conceptualization, funding acquisition, investigation, project administration, resources, supervision, validation, and writing – review and editing. All authors contributed to the article and approved the submitted version. JX: conceptualization, funding acquisition, investigation, project administration, resources, supervision, and writing – review and editing.

Conflicts of interest

There are no conflicts to declare.

Acknowledgements

References

1 J. L. Jimenez, M. R. Canagaratna, N. M. Donahue, A. Prevot and Q. Zhang, Evolution of organic aerosols in the atmosphere, *Science*, 2009, **326**, 1525–1529, DOI: **10.1126/science.1180353**.

2 S. Guo, M. Hu, M. L. Zamora, J. Peng and R. Zhang, Elucidating severe urban haze formation in china, *Proc. Natl. Acad. Sci. U. S. A.*, 2014, **111**(49), 17373, DOI: **10.1073/pnas.1419604111**.

3 C. L. Heald, D. J. Jacob, R. J. Park, L. M. Russell, B. J. Huebert, J. H. Seinfeld, H. Liao and R. J. Weber, A large organic aerosol source in the free troposphere missing from current models, *Geophys. Res. Lett.*, 2005, **32**, L18809, DOI: **10.1029/2005GL023831**.

4 M. Shrivastava, C. D. Cappa, J. Fan, A. H. Goldstein, A. B. Guenther, J. L. Jimenez, C. Kuang, A. Laskin, S. T. Martin, N. L. Ng, T. Petaja, J. R. Pierce, P. J. Rasch, P. Roldin, J. H. Seinfeld, J. Shilling, J. N. Smith, J. A. Thornton, R. Volkamer, J. Wang, D. R. Worsnop, R. A. Zaveri, A. Zelenyuk and Q. Zhang, Recent advances in understanding secondary organic aerosol: implications for global climate forcing, *Rev. Geophys.*, 2017, **55**(2), 509–559, DOI: **10.1002/2016RG000540**.

5 S. Solomon, D. Qin, M. Manning, Z. Chen, M. Marquis, K. Averyt, M. Tignor and H. Miller *Climate Change 2007: the Physical Science Basis. Contribution of Working Group I to the Fourth 16 Assessment Report of the Intergovernmental Panel on Climate Change; Contribution of Working Group I to the Fourth Assesment Report of the Intergovernmental Panel on Climate Change, Climate Change 2007: the Physical Science Basis*, 2013.

6 R. Zhang, G. Li, J. Fan, D. L. Wu and M. J. Molina, Intensification of pacific storm track linked to asian pollution, *Proc. Natl. Acad. Sci. U. S. A.*, 2007, **104**(13), 5295–5299, DOI: **10.1073/pnas.0700618104**.

7 J. Fan, R. Zhang, W.-K. Tao and K. I. Mohr, Effects of aerosol optical properties on deep convective clouds and radiative forcing, *J. Geophys. Res.*, 2008, **113**(D8), D08209, DOI: **10.1029/2007JD009257**.

8 R. Zhang, A. Khalizov, L. Wang, M. Hu and W. Xu, Nucleation and growth of nanoparticles in the atmosphere, *Chem. Rev.*, 2012, **112**(3), 1957–2011, DOI: **10.1021/cr2001756**.

9 H. Henschel, T. Kurtén and H. Vehkamäki, Computational study on the effect of hydration on new particle formation in the sulfuric acid/ammonia and sulfuric acid/dimethylamine systems, *J. Phys. Chem. A*, 2016, **120**(11), 1886–1896, DOI: **10.1021/acs.jpca.5b11366**.

10 D. R. Hanson and F. L. Eisele, Measurement of prenucleation molecular clusters in the NH_3, H_2SO_4, H_2O system, *J. Geophys. Res. Atmos.*, 2002, **107**(D12), 4158, DOI: **10.1029/2001JD001100**.

11 J. Zhao, J. N. Smith, F. L. Eisele, M. Chen, C. Kuang and P. H. McMurry, Observation of neutral sulfuric acid-amine containing clusters in laboratory and ambient measurements, *Atmos. Chem. Phys.*, 2011, **11**(21), 10823–10836, DOI: **10.5194/acp-11-10823-2011**.

12 L. J. Larson, A. Largent and F.-M. Tao, Structure of the sulfuric acid–ammonia system and the effect of water molecules in the gas phase, *J. Phys. Chem. A*, 1999, **103**(34), 6786–6792, DOI: **10.1021/jp991529p**.

13 W. A. Glasoe, K. Volz, B. Panta, N. Freshour, R. Bachman, D. R. Hanson, P. H. McMurry and C. Jen, Sulfuric acid nucleation: an experimental study of the effect of seven bases, *J. Geophys. Res. Atmos.*, 2015, **120**(5), 1933–1950, DOI: **10.1002/2014JD022730**.

14 J. H. Zollner, W. A. Glasoe, B. Panta, K. K. Carlson, P. H. McMurry and D. R. Hanson, Sulfuric acid nucleation: power dependencies, variation with relative humidity, and effect of bases, *Atmos. Chem. Phys.*, 2012, **12**(10), 4399–4411, DOI: **10.5194/acp-12-4399-2012**.

15 A. Kürten, S. Münch, L. Rondo, F. Bianchi, J. Duplissy, T. Jokinen, H. Junninen, N. Sarnela, S. Schobesberger, M. Simon, M. Sipilä, J. Almeida, A. Amorim, J. Dommen, N. M. Donahue, E. M. Dunne, R. C. Flagan, A. Franchin, J. Kirkby, A. Kupc, V. Makhmutov, T. Petäjä, A. P. Praplan, F. Riccobono, G. Steiner, A. Tomé, G. Tsagkogeorgas, P. E. Wagner, D. Wimmer, U. Baltensperger, M. Kulmala, D. R. Worsnop and J. Curtius, Thermodynamics of the formation of sulfuric acid dimers in the binary (H_2SO_4–H_2O) and ternary (H_2SO_4–H_2O–NH_3) system, *Atmos. Chem. Phys.*, 2015, **15**(18), 10701–10721, DOI: **10.5194/acp-15-10701-2015**.

16 C. Kuang, M. Chen, J. Zhao, J. Smith, P. H. McMurry and J. Wang, Size and time-resolved growth rate measurements of 1 to 5 nm freshly formed atmospheric nuclei, *Atmos. Chem. Phys.*, 2012, **12**(7), 3573–3589, DOI: **10.5194/acp-12-3573-2012**.

17 J. Tröstl, K. Chuang, H. Gordon, M. Heinritzi, C. Yan, U. Molteni, L. Ahlm, C. Frege, F. Bianchi, M. Simon, K. Lehtipalo, C. Williamson, S. Craven, J. Duplissy, A. Adamov, J. Almeida, A.-K. Bernhammer,

M. Breitenlechner, S. Brilke, A. Dias, S. Ehrhart, C. Flagan, A. Franchin, C. Fuchs, R. Guida, M. Gysel, A. Hansel, R. Hoyle, T. Jokinen, H. Junninen, J. Kangasluoma, H. Keskinen, J. Kim, M. Krapf, A. Kürten, A. Laaksonen, M. Lawler, M. Leiminger, S. Mathot, O. Möhler, T. Nieminen, A. Onnela, T. Petäjä, M. Piel, P. Miettinen, P. Rissanen, L. Rondo, N. Sarnela, S. Schobesberger, K. Sengupta, M. Sipilä, N. Smith, G. Steiner, A. Tomè, A. Virtanen, C. Wagner, E. Weingartner, D. Wimmer, M. Winkler, P. Ye, S. Carslaw, J. Curtius, J. Dommen, J. Kirkby, M. Kulmala, I. Riipinen, R. Worsnop, M. Donahue and U. Baltensperger, The role of low-volatility organic compounds in initial particle growth in the atmosphere, *Nature*, 2015, 527–531.

18 A. Metzger, B. Verheggen, J. Dommen, J. Duplissy, A. S. H. Prevot, E. Weingartner, I. Riipinen, M. Kulmala, D. V. Spracklen, K. S. Carslaw and U. Baltensperger, Evidence for the role of organics in aerosol particle formation under atmospheric conditions, *Proc. Natl. Acad. Sci. U. S. A.*, 2010, **107**(15), 6646–6651, DOI: **10.1073/pnas.0911330107**.

19 J. Elm, Clusteromics i: principles, protocols, and applications to sulfuric acid-base cluster formation, *ACS Omega*, 2021, **6**(11), 7804–7814, DOI: **10.1021/acsomega.1c00306**.

20 Y. Ling, Y. Wang, J. Duan, X. Xie, Y. Liu, Y. Peng, L. Qiao, T. Cheng, S. Lou, H. Wang, X. Li and X. Xing, Long-term aerosol size distributions and the potential role of volatile organic compounds (VOCs) in new particle formation events in shanghai, *Atmos. Environ.*, 2019, **202**, 345–356, DOI: **10.1016/j.atmosenv.2019.01.018**.

21 M. J. Apsokardu and M. V. Johnston, Nanoparticle growth by particle-phase chemistry, *Atmos. Chem. Phys.*, 2018, **18**(3), 1895–1907, DOI: **10.5194/acp-18-1895-2018**.

22 X. Fang, M. Hu, D. Shang, R. Tang, L. Shi, T. Olenius, Y. Wang, H. Wang, Z. Zhang, S. Chen, X. Yu, W. Zhu, S. Lou, Y. Ma, X. Li, L. Zeng, Z. Wu, J. Zheng and S. Guo, Observational evidence for the involvement of dicarboxylic acids in particle nucleation, *Environ. Sci. Technol. Lett.*, 2020, **7**(6), 388–394, DOI: **10.1021/acs.estlett.0c00270**.

23 P. Roldin, M. Ehn, T. Kurtén, T. Olenius, M. P. Rissanen, N. Sarnela, J. Elm, P. Rantala, L. Hao, N. Hyttinen, L. Heikkinen, D. R. Worsnop, L. Pichelstorfer, C. Xavier, P. Clusius, E. Öström, T. Petäjä, M. Kulmala, H. Vehkamäki, A. Virtanen, I. Riipinen and M. Boy, The role of highly oxygenated organic molecules in the boreal aerosol-cloud-climate system, *Nat. Commun.*, 2019, **10**(1), 4370, DOI: **10.1038/s41467-019-12338-8**.

24 H. B. Singh *Composition Chemistry, and Climate of the Atmosphere*, 1995.

25 A. P. Altshuller, Review: natural volatile organic substances and their effect on air quality in the United States, *Atmos. Environ.*, 1983, **17**(11), 2131–2165, DOI: **10.1016/0004-6981(83)90211-1**.

26 N. Barbara, B. Ian and B. Karl-Heinz, Product study and mechanisms of the reactions of α-pinene and of pinonaldehyde with oh radicals, *J. Geophys. Res. Atmos.*, 1999, **104**(D19), 23645–23656, DOI: **10.1029/1999jd900778**.

27 R. Kamens, M. Jang, C. J. Chien and K. Leach, Aerosol formation from the reaction of α-pinene and ozone using a gas-phase kinetics-aerosol partitioning model, *Environ. Sci. Technol.*, 1999, **33**(9), 1430–1438, DOI: **10.1021/es980725r**.

28 M. Jang and R. M. Kamens, Characterization of secondary aerosol from the photooxidation of toluene in the presence of NO_x and 1-propene, *Environ. Sci. Technol.*, 2001, **35**(18), 3626–3639, DOI: **10.1021/es010676+**.

29 P. Carlier, H. Hannachi and G. Mouvier, The chemistry of carbonyl compounds in the atmosphere—a review – ScienceDirect, *Atmos. Environ.*, 1986, **20**(11), 2079–2099, DOI: **10.1016/0004-6981(86)90304-5**.

30 W. Carter, A. M. Winer and J. N. Pitts, Effect of peroxyacetyl nitrate on the initiation of photochemical smog, *Environ. Sci. Technol.*, 1981, **15**(7), 831–834, DOI: **10.1021/es00089a010**.

31 D. Grosjean, E. L. Williams and E. Grosjean, Atmospheric chemistry of isoprene and of its carbonyl products, *Environ. Sci. Technol.*, 1993, **27**(5), 830–840, DOI: **10.1021/es00042a004**.

32 Y. Ji, Q. Shi, Y. Li, T. An, J. Zheng, J. Peng, Y. Gao, J. Chen, G. Li, Y. Wang, F. Zhang, A. L. Zhang, J. Zhao, M. J. Molina and R. Zhang, Carbenium ion-mediated oligomerization of methylglyoxal for secondary organic aerosol formation, *Proc. Natl. Acad. Sci. U. S. A.*, 2020, **117**(24), 13294–13299, DOI: **10.1073/pnas.1912235117**.

33 Y. Li, Y. Ji, J. Zhao, Y. Wang, Q. Shi, J. Peng, Y. Wang, C. Wang, F. Zhang, Y. Wang, J. H. Seinfeld and R. Zhang, Unexpected oligomerization of small α-dicarbonyls for secondary organic aerosol and brown carbon formation, *Environ. Sci. Technol.*, 2021, **55**(8), 4430–4439, DOI: **10.1021/acs.est.0c08066**.

34 C. Wang, X. Chen, Y. Liu, T. Huang and S. Jiang, Theoretical study of the gas-phase hydrolysis of formaldehyde to produce methanediol and its implication to new particle formation, *ACS Omega*, 2023, **8**(17), 15467–15478, DOI: **10.1021/acsomega.3c00770**.

35 K. Shashikala, P. M. Niha, J. Aswathi, J. Sharanya and D. Janardanan, Theoretical exploration of new particle formation from glycol aldehyde in the atmosphere – a temperature-dependent study, *Comput. Theor. Chem.*, 2023, **1222**, 114057, DOI: **10.1016/j.comptc.2023.114057**.

36 F.-Y. Bai, T.-X. Chi, X.-H. Liu, T.-T. Meng, S. Ni and Z. Zhao, Metal-free catalysis on the reactions of nitric acid with aliphatic aldehydes: a new potential source of organic nitrates, *Atmos. Environ.*, 2023, **299**, 119673, DOI: **10.1016/j.atmosenv.2023.119673**.

37 X. Shi, R. Zhang, Y. Sun, F. Xu, Q. Zhang and W. Wang, A Density functional theory study of aldehydes and their atmospheric products participating in nucleation, *Phys. Chem. Chem. Phys.*, 2018, **20**(2), 1005–1011, DOI: **10.1039/C7CP06226E**.

38 C.-Y. Wang, S. Jiang, Z.-Q. Wang, Y.-R. Liu, H. Wen, T. Huang, Y.-J. Han and W. Huang, Can formaldehyde

contribute to atmospheric new particle formation from sulfuric acid and water?, *Atmos. Environ.*, 2019, **201**, 323–333, DOI: **10.1016/j.atmosenv.2018.12.057**.

39 B. Long, Y. Xia and D. G. Truhlar, Quantitative Kinetics of HO_2 reactions with aldehydes in the atmosphere: high-order dynamic correlation, anharmonicity, and falloff effects are all important, *J. Am. Chem. Soc.*, 2022, **144**(43), 19910–19920, DOI: **10.1021/jacs.2c07994**.

40 J. Liggio, Reactive uptake of glyoxal by particulate matter, *J. Geophys. Res.*, 2005, **110**(D10), D10304, DOI: **10.1029/2004JD005113**.

41 R. Volkamer, F. San Martini, L. T. Molina, D. Salcedo, J. L. Jimenez and M. J. Molina, A missing sink for gas-phase glyoxal in mexico city: formation of secondary organic aerosol, *Geophys. Res. Lett.*, 2007, **34**(19), L19807, DOI: **10.1029/2007GL030752**.

42 R. Volkamer, P. J. Ziemann and M. J. Molina, Secondary organic aerosol formation from acetylene (C_2H_2): seed effect on SOA yields due to organic photochemistry in the aerosol aqueous phase, *Atmos. Chem. Phys.*, 2009, **9**(6), 1907–1928.

43 T.-M. Fu, D. J. Jacob, F. Wittrock, J. P. Burrows, M. Vrekoussis and D. K. Henze, Global budgets of atmospheric glyoxal and methylglyoxal, and implications for formation of secondary organic aerosols, *J. Geophys. Res.*, 2008, **113**(D15), D15303, DOI: **10.1029/2007JD009505**.

44 J. D. Blando and B. J. Turpin, Secondary organic aerosol formation in cloud and fog droplets: a literature evaluation of plausibility, *Atmos. Environ.*, 2000, **34**(10), 1623–1632, DOI: **10.1016/S1352-2310(99)00392-1**.

45 M. Sipila, T. Berndt, T. Petaja, D. Brus, J. Vanhanen, F. Stratmann, J. Patokoski, R. L. Mauldin, A.-P. Hyvarinen, H. Lihavainen and M. Kulmala, The role of sulfuric acid in atmospheric nucleation, *Science*, 2010, **327**(5970), 1243–1246, DOI: **10.1126/science.1180315**.

46 J. Kirkby, J. Curtius, J. Almeida, E. Dunne, J. Duplissy, S. Ehrhart, A. Franchin, S. Gagné, L. Ickes, A. Kürten, A. Kupc, A. Metzger, F. Riccobono, L. Rondo, S. Schobesberger, G. Tsagkogeorgas, D. Wimmer, A. Amorim, F. Bianchi, M. Breitenlechner, A. David, J. Dommen, A. Downard, M. Ehn, R. C. Flagan, S. Haider, A. Hansel, D. Hauser, W. Jud, H. Junninen, F. Kreissl, A. Kvashin, A. Laaksonen, K. Lehtipalo, J. Lima, E. R. Lovejoy, V. Makhmutov, S. Mathot, J. Mikkilä, P. Minginette, S. Mogo, T. Nieminen, A. Onnela, P. Pereira, T. Petäjä, R. Schnitzhofer, J. H. Seinfeld, M. Sipilä, Y. Stozhkov, F. Stratmann, A. Tomé, J. Vanhanen, Y. Viisanen, A. Vrtala, P. E. Wagner, H. Walther, E. Weingartner, H. Wex, P. M. Winkler, K. S. Carslaw, D. R. Worsnop, U. Baltensperger and M. Kulmala, Role of sulphuric acid, ammonia and galactic cosmic rays in atmospheric aerosol nucleation, *Nature*, 2011, **476**(7361), 429–433, DOI: **10.1038/nature10343**.

47 M. Kulmala, J. Kontkanen, H. Junninen, K. Lehtipalo, H. E. Manninen, T. Nieminen, T. Petaja, M. Sipila, S. Schobesberger, P. Rantala, A. Franchin, T. Jokinen, E. Jarvinen, M. Aijala, J. Kangasluoma, J. Hakala, P. P. Aalto, P. Paasonen, J. Mikkila, J. Vanhanen, J. Aalto, H. Hakola, U. Makkonen, T. Ruuskanen, R. L. Mauldin, J. Duplissy, H. Vehkamaki, J. Back, A. Kortelainen, I. Riipinen, T. Kurten, M. V. Johnston, J. N. Smith, M. Ehn, T. F. Mentel, K. E. J. Lehtinen, A. Laaksonen, V.-M. Kerminen and D. R. Worsnop, Direct Observations of atmospheric aerosol nucleation, *Science*, 2013, **339**(6122), 943–946, DOI: **10.1126/science.1227385**.

48 X. Ma, Y. Sun, Z. Huang, Q. Zhang and W. Wang, A density functional theory study of the molecular interactions between a series of amides and sulfuric acid, *Chemosphere*, 2019, **214**, 781–790, DOI: **10.1016/j.chemosphere.2018.08.152**.

49 H. Bardouki, H. Berresheim, M. Vrekoussis, J. Sciare, G. Kouvarakis, K. Oikonomou, J. Schneider and N. Mihalopoulos, Gaseous (DMS, MSA, SO_2, H_2SO_4 and DMSO) and particulate (sulfate and methanesulfonate) sulfur species over the northeastern coast of crete, *Atmos. Chem. Phys.*, 2003, **3**, 1871–1886.

50 C. J. Gaston, R. A. Pratt, X. Qin and K. A. Prather, Real-time detection and mixing state of methanesulfonate in single particles at an inland urban location during a phytoplankton bloom, *Environ. Sci. Technol.*, 2010, **44**(5), 1566–1572, DOI: **10.1021/es902069d**.

51 M. L. Dawson, M. E. Varner, V. Perraud, M. J. Ezell, R. B. Gerber and B. J. Finlayson-Pitts, Simplified mechanism for new particle formation from methanesulfonic acid, amines, and water *via* experiments and *ab initio* calculations, *Proc. Natl. Acad. Sci. U. S. A.*, 2012, **109**(46), 18719–18724, DOI: **10.1073/pnas.1211878109**.

52 M. L. Dawson, M. E. Varner, V. Perraud, M. J. Ezell, J. Wilson, A. Zelenyuk, R. B. Gerber and B. J. Finlayson-Pitts, Amine–amine exchange in aminium–methanesulfonate aerosols, *J. Phys. Chem. C*, 2014, **118**(50), 29431–29440, DOI: **10.1021/jp506560w**.

53 M. J. Ezell, H. Chen, K. D. Arquero and B. J. Finlayson-Pitts, Aerosol fast flow reactor for laboratory studies of new particle formation, *J. Aerosol Sci.*, 2014, **78**, 30–40, DOI: **10.1016/j.jaerosci.2014.08.009**.

54 N. Nishino, K. D. Arquero, M. L. Dawson and B. J. Finlayson-Pitts, Infrared studies of the reaction of methanesulfonic acid with trimethylamine on surfaces, *Environ. Sci. Technol.*, 2014, **48**(1), 323–330, DOI: **10.1021/es403845b**.

55 H. Chen, M. E. Varner, R. B. Gerber and B. J. Finlayson-Pitts, Reactions of methanesulfonic acid with amines and ammonia as a source of new particles in air, *J. Phys. Chem. B*, 2016, **120**(8), 1526–1536, DOI: **10.1021/acs.jpcb.5b07433**.

56 H. Chen, M. J. Ezell, K. D. Arquero, M. E. Varner, M. L. Dawson, R. B. Gerber and B. J. Finlayson-Pitts, New particle formation and growth from methanesulfonic acid, trimethylamine and water, *Phys. Chem. Chem. Phys.*, 2015, **17**(20), 13699–13709, DOI: **10.1039/C5CP00838G**.

57 Y. Hu, S. Chen, S. Ye, S. Wei, B. Chu, R. Wang, H. Li and T. Zhang, The role of trifluoroacetic acid in new particle

formation from methanesulfonic acid-methylamine, *Atmos. Environ.*, 2023, **311**, 120001, DOI: **10.1016/j.atmosenv.2023.120001**.

58 K. D. Arquero, R. B. Gerber and B. J. Finlayson-Pitts, The role of oxalic acid in new particle formation from methanesulfonic acid, methylamine, and water, *Environ. Sci. Technol.*, 2017, **51**(4), 2124–2130, DOI: **10.1021/acs.est.6b05056**.

59 J. S. Johnson and C. N. Jen, Role of methanesulfonic acid in sulfuric acid–amine and ammonia new particle formation, *ACS Earth Space Chem.*, 2023, **7**(3), 653–660, DOI: **10.1021/acsearthspacechem.3c00017**.

60 N. Tsona Tchinda, L. Du, L. Liu and X. Zhang, Pyruvic acid, an efficient catalyst in SO_3 hydrolysis and effective clustering agent in sulfuric-acid-based new particle formation, *Atmos. Chem. Phys.*, 2022, **22**(3), 1951–1963, DOI: **10.5194/acp-22-1951-2022**.

61 S.-H. Lee, H. Gordon, H. Yu, K. Lehtipalo, R. Haley, Y. Li and R. Zhang, New particle formation in the atmosphere: from molecular clusters to global climate, *J. Geophys. Res. Atmos.*, 2019, **124**(13), 7098–7146, DOI: **10.1029/2018JD029356**.

62 M. Kulmala, T. Petäjä, M. Ehn, J. Thornton, M. Sipilä, D. R. Worsnop and V.-M. Kerminen, Chemistry of atmospheric nucleation: on the recent advances on precursor characterization and atmospheric cluster composition in connection with atmospheric new particle formation, *Annu. Rev. Phys. Chem.*, 2014, **65**, 21–37, DOI: **10.1146/annurev-physchem-040412-110014**.

63 M. Peltola, C. Rose, J. V. Trueblood, S. Gray, M. Harvey and K. Sellegri, Chemical precursors of new particle formation in coastal New Zealand, *Atmos. Chem. Phys.*, 2023, **23**(7), 3955–3983, DOI: **10.5194/acp-23-3955-2023**.

64 R. Cai, C. Yan, D. R. Worsnop, F. Bianchi, V.-M. Kerminen, Y. Liu, L. Wang, J. Zheng, M. Kulmala and J. Jiang, An Indicator for sulfuric acid–amine nucleation in atmospheric environments, *Aerosol Sci. Technol.*, 2021, **55**(9), 1059–1069, DOI: **10.1080/02786826.2021.1922598**.

65 A. Ning, H. Zhang, X. Zhang, Z. Li, Y. Zhang, Y. Xu and M. Ge, A molecular-scale study on the role of methanesulfinic acid in marine new particle formation, *Atmos. Environ.*, 2020, **227**, 117378, DOI: **10.1016/j.atmosenv.2020.117378**.

66 E. Dovrou, K. H. Bates, J. M. Moch, L. J. Mickley, D. J. Jacob and F. N. Keutsch, Catalytic role of formaldehyde in particulate matter formation, *Proc. Natl. Acad. Sci. U. S. A.*, 2022, **119**(6), e2113265119, DOI: **10.1073/pnas.2113265119**.

67 M. Jang and R. M. Kamens, Atmospheric secondary aerosol formation by heterogeneous reactions of aldehydes in the presence of a sulfuric acid aerosol catalyst, *Environ. Sci. Technol.*, 2001, **35**(24), 4758–4766, DOI: **10.1021/es010790s**.

68 M. Jang, N. M. Czoschke, S. Lee and R. M. Kamens, Heterogeneous atmospheric aerosol production by acid-catalyzed particle-phase reactions, *Science*, 2002, **298**(5594), 814–817, DOI: **10.1126/science.1075798**.

69 M. Jang, B. Carroll, B. Chandramouli and R. M. Kamens, Particle growth by acid-catalyzed heterogeneous reactions of organic carbonyls on preexisting aerosols, *Environ. Sci. Technol.*, 2003, **37**(17), 3828–3837, DOI: **10.1021/es021005u**.

70 J. Zhao, N. P. Levitt, R. Zhang and J. Chen, Heterogeneous reactions of methylglyoxal in acidic media: implications for secondary organic aerosol formation, *Environ. Sci. Technol.*, 2006, **40**(24), 7682–7687, DOI: **10.1021/es060610k**.

71 M. E. Gomez, Y. Lin, S. Guo and R. Zhang, Heterogeneous chemistry of glyoxal on acidic solutions. an oligomerization pathway for secondary organic aerosol formation, *J. Phys. Chem. A*, 2015, **119**(19), 4457–4463, DOI: **10.1021/jp509916r**.

72 C.-Y. Wang, S. Jiang, Z.-Q. Wang, Y.-R. Liu, H. Wen, T. Huang, Y.-J. Han and W. Huang, Can formaldehyde contribute to atmospheric new particle formation from sulfuric acid and water?, *Atmos. Environ.*, 2019, **201**, 323–333, DOI: **10.1016/j.atmosenv.2018.12.057**.

73 R. J. Weber, P. H. McMurry, F. L. Eisele and D. J. Tanner, Measurement of expected nucleation precursor species and 3–500-Nm diameter particles at mauna loa observatory, Hawaii, *J. Atmos. Sci.*, 1995, **52**(12), 2242–2257, DOI: **10.1175/1520-0469(1995)052<2242:MOENPS>2.0.CO;2**.

74 J. Merikanto, J. Duplissy, A. Määttänen, H. Henschel, N. M. Donahue, D. Brus, S. Schobesberger, M. Kulmala and H. Vehkamäki, Effect of ions on sulfuric acid-water binary particle formation: 1. theory for kinetic- and nucleation-type particle formation and atmospheric implications: binary particle formation theory, *J. Geophys. Res. Atmos.*, 2016, **121**(4), 1736–1751, DOI: **10.1002/2015JD023538**.

75 J. Kirkby, J. Curtius, J. Almeida, E. Dunne, J. Duplissy, S. Ehrhart, A. Franchin, S. Gagné, L. Ickes, A. Kürten, A. Kupc, A. Metzger, F. Riccobono, L. Rondo, S. Schobesberger, G. Tsagkogeorgas, D. Wimmer, A. Amorim, F. Bianchi, M. Breitenlechner, A. David, J. Dommen, A. Downard, M. Ehn, R. C. Flagan, S. Haider, A. Hansel, D. Hauser, W. Jud, H. Junninen, F. Kreissl, A. Kvashin, A. Laaksonen, K. Lehtipalo, J. Lima, E. R. Lovejoy, V. Makhmutov, S. Mathot, J. Mikkilä, P. Minginette, S. Mogo, T. Nieminen, A. Onnela, P. Pereira, T. Petäjä, R. Schnitzhofer, J. H. Seinfeld, M. Sipilä, Y. Stozhkov, F. Stratmann, A. Tomé, J. Vanhanen, Y. Viisanen, A. Vrtala, P. E. Wagner, H. Walther, E. Weingartner, H. Wex, P. M. Winkler, K. S. Carslaw, D. R. Worsnop, U. Baltensperger and M. Kulmala, Role of sulphuric acid, ammonia and galactic cosmic rays in atmospheric aerosol nucleation, *Nature*, 2011, **476**(7361), 429–433, DOI: **10.1038/nature10343**.

76 J. Almeida, S. Schobesberger, A. Kürten, I. K. Ortega, O. Kupiainen-Määttä, A. P. Praplan, A. Adamov, A. Amorim, F. Bianchi, M. Breitenlechner, A. David, J. Dommen, N. M. Donahue, A. Downard, E. Dunne, J. Duplissy, S. Ehrhart, R. C. Flagan, A. Franchin, R. Guida, J. Hakala, A. Hansel, M. Heinritzi, H. Henschel, T. Jokinen, H. Junninen, M. Kajos, J. Kangasluoma, H. Keskinen, A. Kupc, T. Kurtén, A. N. Kvashin,

A. Laaksonen, K. Lehtipalo, M. Leiminger, J. Leppä, V. Loukonen, V. Makhmutov, S. Mathot, M. J. McGrath, T. Nieminen, T. Olenius, A. Onnela, T. Petäjä, F. Riccobono, I. Riipinen, M. Rissanen, L. Rondo, T. Ruuskanen, F. D. Santos, N. Sarnela, S. Schallhart, R. Schnitzhofer, J. H. Seinfeld, M. Simon, M. Sipilä, Y. Stozhkov, F. Stratmann, A. Tomé, J. Tröstl, G. Tsagkogeorgas, P. Vaattovaara, Y. Viisanen, A. Virtanen, A. Vrtala, P. E. Wagner, E. Weingartner, H. Wex, C. Williamson, D. Wimmer, P. Ye, T. Yli-Juuti, K. S. Carslaw, M. Kulmala, J. Curtius, U. Baltensperger, D. R. Worsnop, H. Vehkamäki and J. Kirkby, Molecular understanding of sulphuric acid–amine particle nucleation in the atmosphere, *Nature*, 2013, **502**(7471), 359–363, DOI: 10.1038/nature12663.

77 O. Kupiainen, I. K. Ortega, T. Kurtén and H. Vehkamäki, Amine substitution into sulfuric acid – ammonia clusters, *Atmos. Chem. Phys.*, 2012, **12**(8), 3591–3599, DOI: 10.5194/acp-12-3591-2012.

78 M. Liu, N. Myllys, Y. Han, Z. Wang, L. Chen, W. Liu and J. Xu, Microscopic insights into the formation of methanesulfonic acid–methylamine–ammonia particles under acid-rich conditions, *Front. Ecol. Evol.*, 2022, **10**, 875585, DOI: 10.3389/fevo.2022.875585/full.

79 V. Perraud, J. Xu, R. B. Gerber and B. J. Finlayson-Pitts, Integrated experimental and theoretical approach to probe the synergistic effect of ammonia in methanesulfonic acid reactions with small alkylamines, *Environ. Sci.: Processes Impacts*, 2020, **22**(2), 305–328, DOI: 10.1039/C9EM00431A.

80 *Nucleophilic Addition Reaction – General Mechanism, Examples*. https://chem.libretexts.org/Bookshelves/Introductory_Chemistry/Introduction_to_Organic_and_Biochemistry_(Malik)/04%3A_Organic_reactions/4.06%3A_Nucleophilic_Addition_Reactions#:~:text=The%20addition%20of%20alcohol%20(R,as%20in%20the%20following%20example.

81 *19.4: Nucleophilic Addition Reactions of Aldehydes and Ketones. Chemistry LibreTexts*. https://chem.libretexts.org/Bookshelves/Organic_Chemistry/Organic_Chemistry_(McMurry)/19%3A_Aldehydes_and_Ketones-_Nucleophilic_Addition_Reactions/19.04%3A_Nucleophilic_Addition_Reactions_of_Aldehydes_and_Ketones.

82 J. Zhang and M. Dolg, ABCluster: the artificial bee colony algorithm for cluster global optimization, *Phys. Chem. Chem. Phys.*, 2015, **17**, 24173–24181, DOI: 10.1039/c5cp04060d.

83 J. Zhang and M. Dolg, Global optimization of clusters of rigid molecules using the artificial bee colony algorithm, *Phys. Chem. Chem. Phys.*, 2016, **18**, 3003–3010, DOI: 10.1039/c5cp04060d.

84 D. Karaboga, *An Idea Based on Honey Bee Swarm for Numerical Optimization*, 2005.

85 J. Stewart, Optimization of parameters for semiempirical methods v: modification of NDDO approximations and application to 70 elements, *J. Mol. Model.*, 2007, **13**(12), 1173–1213, DOI: 10.1007/s00894-007-0233-4.

86 J. Hostaš, J. Řezáč and P. Hobza, On the performance of the semiempirical quantum mechanical PM6 and PM7 methods for noncovalent interactions, *Chem. Phys. Lett.*, 2013, **568–569**, 161–166, DOI: 10.1016/j.cplett.2013.02.069.

87 A. Ning and X. Zhang, The synergistic effects of methanesulfonic acid (MSA) and methanesulfinic acid (MSIA) on marine new particle formation, *Atmos. Environ.*, 2022, **269**, 118826, DOI: 10.1016/j.atmosenv.2021.118826.

88 D. Chen, W. Wang, D. Li and W. Wang, Atmospheric implication of synergy in methanesulfonic acid–base trimers: a theoretical investigation, *RSC Adv.*, 2020, **10**(9), 5173–5182, DOI: 10.1039/C9RA08760E.

89 N. Myllys, D. Myers, S. Chee and J. N. Smith, Molecular properties affecting the hydration of acid–base clusters, *Phys. Chem. Chem. Phys.*, 2021, **23**(23), 13106–13114, DOI: 10.1039/D1CP01704G.

90 J. P. Perdew, J. A. Chevary, S. H. Vosko, K. A. Jackson, M. R. Pederson, D. J. Singh and C. Fiolhais, Atoms, molecules, solids, and surfaces: applications of the generalized gradient approximation for exchange and correlation, *Phys. Rev. B: Condens. Matter Mater. Phys.*, 1992, **46**(11), 6671–6687, DOI: 10.1103/PhysRevB.46.6671.

91 R. G. Parr and Y. Weitao, *Density-Functional Theory of Atoms and Molecules*, Oxford University Press, 1995. DOI: 10.1093/oso/9780195092769.001.0001.

92 A. D. Becke, Density-functional thermochemistry. III. The role of exact exchange, *J. Chem. Phys.*, 1993, **98**(7), 5648–5652, DOI: 10.1063/1.464913.

93 S. Grimme, J. Antony, S. Ehrlich and H. Krieg, A consistent and accurate *ab initio* parametrization of density functional dispersion correction (DFT-D) for the 94 elements H-Pu, *J. Chem. Phys.*, 2010, **132**(15), 154104, DOI: 10.1063/1.3382344.

94 M. J. Frisch, M. Head-Gordon and J. A. Pople, A direct MP2 gradient method, *Chem. Phys. Lett.*, 1990, **166**(3), 275–280, DOI: 10.1016/0009-2614(90)80029-D.

95 M. Head-Gordon, J. A. Pople and M. J. Frisch, MP2 energy evaluation by direct methods, *Chem. Phys. Lett.*, 1988, **153**(6), 503–506, DOI: 10.1016/0009-2614(88)85250-3.

96 M. J. Frisch, M. Head-Gordon and J. A. Pople, Semi-direct algorithms for the MP2 energy and gradient, *Chem. Phys. Lett.*, 1990, **166**(3), 281–289, DOI: 10.1016/0009-2614(90)80030-H.

97 J. P. Foster and F. Weinhold, Natural hybrid orbitals, *J. Am. Chem. Soc.*, 1980, **102**(24), 7211–7218, DOI: 10.1021/ja00544a007.

98 A. E. Reed and F. Weinhold, Natural bond orbital analysis of near-hartree–fock water dimer, *J. Chem. Phys.*, 1983, **78**(6), 4066–4073, DOI: 10.1063/1.445134.

99 M. J. Frisch, G. W. Trucks, H. B. Schlegel, G. E. Scuseria, M. A. Robb, and J. R. Cheeseman. *Gaussian 16, Revision A.03*, Gaussian, Inc, Wallingford, CT, https://gaussian.com/citation_a03/, accessed 21 January 2022.

100 T. Takayanagi, T. Yoshikawa, A. Kakizaki, M. Shiga and M. Tachikawa, Molecular dynamics simulations of small glycine–$(H_2O)_n$ (N=2–7) clusters on semiempirical PM6 potential energy surfaces, *J. Mol. Struct. Theochem*, 2008, **869**(1–3), 29–36, DOI: **10.1016/j.theochem.2008.08.016**.

101 R. D. Tosso, S. A. Andujar, L. Gutierrez, E. Angelina, R. Rodríguez, M. Nogueras, H. Baldoni, F. D. Suvire, J. Cobo and R. D. Enriz, Molecular modeling study of dihydrofolate reductase inhibitors. molecular dynamics simulations, quantum mechanical calculations, and experimental corroboration, *J. Chem. Inf. Model.*, 2013, **53**(8), 2018–2032, DOI: **10.1021/ci400178h**.

102 M. Wang, Y. Mei and U. Ryde, Host–guest relative binding affinities at density-functional theory level from semiempirical molecular dynamics simulations, *J. Chem. Theory Comput.*, 2019, **15**(4), 2659–2671, DOI: **10.1021/acs.jctc.8b01280**.

103 J. VandeVondele, M. Krack, F. Mohamed, M. Parrinello, T. Chassaing and J. Hutter, Quickstep: fast and accurate density functional calculations using a mixed Gaussian and plane waves approach, *Comput. Phys. Commun.*, 2005, **167**(2), 103–128, DOI: **10.1016/j.cpc.2004.12.014**.

104 S. Nosé, A unified formulation of the constant temperature molecular dynamics methods, *J. Chem. Phys.*, 1984, **81**(1), 511–519, DOI: **10.1063/1.447334**.

105 W. G. Hoover, Canonical dynamics: equilibrium phase-space distributions, *Phys. Rev. A: At., Mol., Opt. Phys.*, 1985, **31**(3), 1695–1697, DOI: **10.1103/PhysRevA.31.1695**.

106 E. R. Johnson, S. Keinan, P. Mori-Sanchez, J. Contreras-Garcia, A. J. Cohen and W. Yang, Revealing noncovalent interactions, *J. Am. Chem. Soc.*, 2010, **132**(18), 6498, DOI: **10.1021/ja100936w**.

107 E. R. Johnson, S. Keinan, P. Mori-Sánchez, J. Contreras-García, A. J. Cohen and W. Yang, Revealing noncovalent interactions, *J. Am. Chem. Soc.*, 2010, **132**(18), 6498–6506, DOI: **10.1021/ja100936w**.

108 W. Humphrey, A. Dalke and K. Schulten, VMD: visual molecular dynamics, *J. Mol. Graphics*, 1996, **14**(1), 33–38, DOI: **10.1016/0263-7855(96)00018-5**.

109 University of Illinois, *Visual Molecular Dynamics*, 2014.

110 *19.5: Nucleophilic Addition of Water – Hydration. Chemistry LibreTexts*, **https://chem.libretexts.org/Bookshelves/Organic_Chemistry/Organic_Chemistry_(McMurry)/19%3A_Aldehydes_and_Ketones-_Nucleophilic_Addition_Reactions/19.05%3A_Nucleophilic_Addition_of_Water-_Hydration**.